KEK CP-030
INP MSU Preprint-95-16/380
14 June 1995

Probing the H^3 vertex in e^+e^-, γe and $\gamma\gamma$ collisions for light and intermediate Higgs bosons

V.A. Ilyin[1], A.E. Pukhov[2]
Institute of Nuclear Physics, Moscow State University, 119899 Moscow, RUSSIA

Y. Kurihara[3], Y. Shimizu[4]
National Laboratory for High Energy Physics (KEK), Tsukuba, Ibaraki 305, JAPAN

T. Kaneko[5]
Laboratoire d'Annecy-le-Vieux de Physique des Particules (LAPP), B.P. 110, F-74941 Annecy-le-Vieux Cedex, FRANCE

Abstract

We have studied double Higgs production at future linear colliders while paying special attention to the option of high-energy and high-luminosity photon beams. The main purpose was to examine the feasibility of e^+e^-, γe and $\gamma\gamma$ colliders in order to probe the anomalous triple Higgs coupling, which is crucial for understanding the Standard Model. We considered mainly the cases of light and intermediate Higgs bosons. Double Higgs production is almost background free, except in the $M_H \sim M_Z$ mass range, which is discussed separately. It is shown that for a light Higgs boson the H^3 coupling can be measured even at e^+e^- collider at 500 GeV. For a intermediate Higgs boson a collider in the TeV region is suitable for such an investigation. We have estimated the bounds on the anomalous H^3 coupling, which can be experimentally established using future linear colliders.

[1]ilyin@theory.npi.msu.su
[2]pukhov@theory.npi.msu.su
[3]kurihara@kekvax.kek.jp
[4]shimiz@minami.kek.jp
[5]kaneko@minami.kek.jp, On leave of absence from Meiji-Gakuin University, Kamikurata, Totsuka 244, JAPAN.

1 Introduction

One of the most important problems after the Higgs boson is discovered in the future will be to study its self-interaction. It is necessary to clarify the nature of the spontaneous breaking of the gauge symmetry which provides nonzero masses of intermediate bosons and fermions. In the Standard Model (SM) one scalar Higgs doublet field is introduced,

$$\Phi \;=\; \frac{1}{\sqrt{2}} \left(\begin{array}{c} H + \upsilon + i\phi_3 \\ -\phi_2 - i\phi_1 \end{array} \right).$$

Here, H is the physical scalar boson (the Higgs boson, itself) and the ϕ_i's are unphysical Goldstone fields corresponding to pure gauge degrees of freedom. The Higgs potential is $SU(2)$ invariant,

$$V(\Phi^*\Phi) \;=\; \lambda(\Phi^*\Phi - \frac{1}{2}\upsilon^2)^2, \qquad \upsilon = \frac{2M_W \sin\theta_W}{e}. \tag{1}$$

Here, $e = \sqrt{4\pi\alpha}$ is the electric charge, M_W the mass of W boson and θ_W the Weinberg mixing angle. The value of the vacuum expectation, $\upsilon \approx 250$ GeV, is fixed by the parameters of the intermediate bosons obtained from the experiments. The coupling constant (λ) is a free parameter in SM and is associated with the Higgs mass,

$$\lambda \;=\; \frac{\pi\alpha}{4} \frac{M_H^2}{\sin^2\theta_W M_W^2}.$$

The experimental bound on the Higgs mass is now $M_H > 64.5$ GeV [1]. The region $M_H < 90$ GeV (*light* Higgs) will be explored by LEP200 experiments while the mass range up to 400 GeV (*intermediate* Higgs, $M_H < 2M_Z$, and heavier) can be scanned at future linear colliders with $\sqrt{s} = 500$ GeV (discussed intensively these days [2]).

In SUSY extensions of SM (see, for example, [3, 4] and references therein) several scalar particles are predicted to have the lightest mass, less than 200 GeV. The hypothesis of grand unification theories also requires such light Higgs boson in order to provide the experimental value of $\sin\theta_W$. Experiments at LEP200 and future linear colliders will crucially expose these intriguing theoretical constructions. Hence, in the situation where only one scalar boson is discovered, a search for evidence of a nonminimal Higgs self-interaction becomes an actual problem. Such evidence could be deviations of H^3 and H^4 couplings from their SM values and contributions of higher order vertices (H^n, $n > 4$). Unfortunately, direct experimental probing of the vertices of H^4 and higher order is impossible, even at the presently discussed colliders, because of cross sections that are too small. A measurement of the triple Higgs coupling is thus the only possibility to confirm the SM structure and to select new theories.

The H^3 vertex also contributes to single H production, which is discussed as discovery reactions. However, in these processes the interaction contains *Higgs-light fermion* vertex, which has negligibly small coupling constant. So the H^3 vertex contribution to these reactions is very small. Furthermore, single H production reactions of higher orders (α^n, $n \geq 5$) have very small cross sections. As a result, *the processes of order α^3 and α^4 with double Higgs production* are practically the only way to investigate a Higgs self-interaction.

For this purpose, $e\gamma$ and $\gamma\gamma$ colliders (*Photon Linear Colliders* – PLC), which are based on the idea of Compton backscattering of laser photons against the electron beam [5, 6], are useful tools as well as e^+e^- colliders are. The energy distribution of the backscattered photons generally has a wide spectrum. If it is possible, however, to shift the interaction point far enough

from the conversion point, the low-energy photons will exit the interaction area due to relatively large escape angles. The photon beam can be made practically monochromatic (peaked at a point close to the energy of a basic electron beam, $E_\gamma^{max} \sim 0.8E_e$) in this way. Moreover, when the polarization of laser photons and that of electrons are opposite, the spectrum of backscattered photons will be most monochromatic. Our analysis is based on the cross sections for a monochromatic beam. It is expected that the luminosity of PLC could be on the same order as that for an e^+e^- collider [7], which is expected to be up to $100\,\mathrm{fb}^{-1}/year$. We also estimate decreasing cross sections resulting from a convolution with the whole energy spectrum of the backscattered photon (we used formulas given in [5]).

Electron beams can be highly polarized at future linear colliders [12]. A polarized positron beam has also been proposed [13], though there are still technical difficulties. Since the polarized positron beam is important, anyway, we also mention the polarization of the positron beam. A high rate of circular polarization of photon beams will also be available. For e^+e^- and γe processes, the total cross sections crucially depend on electron and positron chirality. The effective luminosity can be enhanced by using polarized beams. This enhancement could be important because much higher statistics are needed for some physically interesting processes, such as the double Higgs production. Keeping this circumstance in mind, we note that in γ processes, which we consider here, there is no significant dependence on the polarization of photons. However, for e^+e^- and γe processes, the cross sections in the case of polarized electrons gives just twice (or more when the positron beam is also polarized) that of the unpolarized one. We then basically estimate unpolarized results, and some comments about a polarization dependence of the cross sections are given, if necessary.

The paper is organized as follows. In section 2 parametrization of an anomalous Higgs potential is introduced. In section 3 we present numerical results for processes and some comments on signals produced along with double Higgs production. Those in e^+e^- collisions have been analyzed in [14]-[16]. In the present work we confirm their numerical results in e^+e^- collisions (Sec.3.1) and give new results for γe (Sec.3.2) and $\gamma\gamma$ (Sec.3.3) collisions. We pay special attention to the case $M_H \approx M_Z$, including a background analysis concerning the discussed processes in section 3.4. In section 4 we give an analysis of the dependence of the cross sections on anomalous H^3 coupling for considered processes in e^+e^-, γe and $\gamma\gamma$ collisions.

2 Anomalous Higgs potential

To estimate the contribution of the triple Higgs vertex we have to change the corresponding constant λ in the Higgs potential (1) while keeping the $SU(2)$ invariance as well as the value of the vacuum expectation. We thus add to the SM potential the following monomials [17]:

$$V_n(\Phi^*\Phi) \;\equiv\; \frac{\lambda_n}{n!}(2\Phi^*\Phi - \upsilon^2)^n, \qquad n = 3, 4, \ldots$$

Although many new vertices will appear, for those processes of order α^3 and α^4 only some of them can contribute. They are

$$V_3^{(3)+(4)} \;=\; \frac{\lambda_3}{6}(8\upsilon^3H^3 + 12\upsilon^2H^4 + 12\upsilon^2H^2\phi_3^2 + 24\upsilon^2H^2\omega^+\omega^-), \tag{2}$$

$$V_4^{(3)+(4)} \;=\; \frac{2\lambda_4}{3}\upsilon^4H^4. \tag{3}$$

where $\omega^{\pm} = (\phi_1 \mp i\phi_2)/\sqrt{2}$.

In the unitary gauge, where $\phi_i = 0$, this new potential changes only two SM vertices, H^3 and H^4, and results in new free parameters, $\lambda_{3,4}$. In other gauges, for example in renormalizable covariant gauges, all vertices (2,3) can contribute, again with two free parameters. Note that the constant at the H^4 vertex stays a free parameter for $O(\alpha^3)$ and $O(\alpha^4)$ processes. Unfortunately λ_4 is out of the experimental study due to small cross sections for possible processes and only λ_3 coupling can be seen.

We now introduce the following dimensionless parameter:

$$\delta \equiv \frac{8v^4}{3M^2}\lambda_3.$$

The value $\delta = -1$ corresponds to the vanishing H^3 vertex.

It is clear that the cross sections are of quadratic form in δ,

$$\sigma(\delta) = \kappa(\delta - \delta_0)^2 + \sigma(\delta_0).$$

Here, δ_0 corresponds to the minimum of this function. To determine the function $\sigma(\delta)$ we calculate three points at $\delta = \pm 1, 0$, where $\delta = 0$ implies SM.

Since the cross section is a quadratic function of δ, any analysis to derive an anomalous coupling would be slightly complicated. We now consider a statistical analysis when the experiment does not show any deviation from SM at the 95% CL for H^3 coupling. This means that $|N(\delta) - N(0)| < 1.96\sqrt{N(0)}$, where $N(\delta) = \mathcal{L}\sigma(\delta)$ is the number of detected events and $\mathcal{L}$ is the integrated luminosity. Two variants are possible:

(A) if $\delta_0^2 > D^2$, then

$$\delta_0 - \sqrt{\delta_0^2 + D^2} < \delta < \delta_0 - \sqrt{\delta_0^2 - D^2} \qquad or \qquad \delta_0 + \sqrt{\delta_0^2 - D^2} < \delta < \delta_0 + \sqrt{\delta_0^2 + D^2}; \tag{4}$$

(B) if $\delta_0^2 < D^2$, then

$$\delta_0 - \sqrt{\delta_0^2 + D^2} < \delta < \delta_0 + \sqrt{\delta_0^2 + D^2}. \tag{5}$$

Here,

$$D^2 = \frac{1.96\sqrt{\sigma(0)}}{\kappa\sqrt{\mathcal{L}}}.$$

Variant (A) implies that two values of δ correspond to the measured cross section (within experimental errors). Furthermore, these two values are separated by fixed interval which does not depend on the experimental errors. This discrete uncertainty takes place even if the number of measured events is sufficient to the level predicted by SM – some *shadow* interval will show up! When the luminosity is small, variant (B) is realised. However, with increasing the integrated luminosity a discrete uncertainty appears at some critical integrated luminosity. It depends on only the Higgs mass, and equals

$$\hat{\mathcal{L}} = \left(\frac{1.96}{\delta_0^2}\right)^2 \frac{\sigma(0)}{\kappa^2}.$$

To characterize the dependence on δ we use two parameters which we denote as $\delta^{\pm}$. In case (B) these parameters are the corresponding bounds in (5). In case (A) they are the bounds of either of the intervals in (4) that includes the SM point $\delta = 0$.

We cannot expect that the statistics for double Higgs-production reactions could be high. In some cases, therefore, when the number of events is around seven or less, the distribution of the event probability will be Poisson rather than Gaussian. Nevertheless, for definiteness we use the formulas given above.

3 Double Higgs production cross sections

In this section we present numerical results for some processes with double Higgs production. We carried out the calculations using the framework of the Standard Model. We used CompHEP [19] and GRACE [20] (see also [21]) packages for independent calculations of the matrix elements and cross sections. These packages provide automatic computation of the cross sections and distributions in the Standard Model as well as its extensions at the tree level. All processes were estimated, including a complete set of diagrams. The calculations were made with 1% accuracy, and both packages gave consistent results. Numerical results were obtained with the following values of physical constants: $\alpha = 1/128$, $M_Z = 91.178$ GeV, $\sin\theta_W = 0.474$.

The values of total cross sections are collected in the Table 1. In Fig. 1 we show the energy dependence of the total cross sections and in Fig. 2 the corresponding Higgs mass dependence.

3.1 e^+e^- collisions

a) $e^+e^- \longrightarrow ZHH$. This process has been investigated in [14, 15]; we also confirmed their numerical results. Here, Higgs bosons are produced via bremsstrahlung from the Z boson (see Fig. 3). The cross section decreases with energy far enough from the threshold. At some energy the total cross section has its maximum value of σ^{tot}_{max}, depending on the Higgs mass. Higgs and Z bosons escape at large angles and with practically the same distributions. Fig. 4 gives angular distribution for the Higgs boson. Since fermion chirality is conserved at the *Z-fermion* vertex, the rate of this reaction may increase by practically twice when electrons and positrons are polarized.

For this reaction there is no competitive background. A light Higgs boson decays to a $b\bar{b}$-pair (more than 90%) and other fermion pairs. For $M_H > 150$ GeV the Higgs boson decays mainly into WW or ZZ. For $M_H < 150$ GeV the main branchings are $ZHH \to Zb\bar{b}b\bar{b} \to 6\,jets$, and $ZHH \to ZWWWW \to 10\,jets$ for heavier Higgs bosons. In these cases suitable cuts on the invariant masses should be introduced around those points corresponding to M_H, M_Z and M_W. We can say that for light Higgs the observation of more than 5 events per year is plausible at a 500-GeV e^+e^- collider with $\mathcal{L} = 10\,\mathrm{fb}^{-1}/year$. The initial state radiation would reduce 7% of the total cross section. To study a heavier Higgs boson, an operation at the cross section maximum is needed to obtain sufficient statistics.

b) $e^+e^- \longrightarrow \bar{\nu}_e\nu_e HH$. This process was investigated in [16]. Our numerical results are in agreement with this work. In this reaction diagrams with the WW fusion (see Fig. 5) give the main contribution. The total cross section increases with energy. In Fig. 4 we give an angular distribution for Higgs bosons which is smooth with two peaks at $\theta_H \sim 10^\circ$ and 170°. This reaction has the biggest cross section among other processes within the discussed Higgs mass range.

The final states are identified by the decay of Higgs bosons. The main signature for $M_H < 150$ GeV is four jets. For larger masses this is four gauge bosons ($WWWW$, $WWZZ$, $ZZZZ$) with their subsequent decays, whose invariant mass distribution shows a peak at M_H. The

possible background could be the reaction $e^+e^- \to HH$, which proceeds at the one-loop level. It seems, however, that its cross section is very small. In [22] it is estimated to be less than 0.05 fb at $\sqrt{s} = 250$ GeV and $M_H = 100$ GeV, and with visible decreasing at high $\sqrt{s}$.

Since only a left-handed electron and a right-handed positron contribute in this reaction, if the electron beam (both electron and positron beams) would be polarized, the statistics would be increased by twice (four times, respectively). For unpolarized experiments 34 events per year are produced for $M_H = 150$ GeV at $\sqrt{s} = 2$ TeV and $\mathcal{L} = 100\,\mathrm{fb}^{-1}/year$. The initial state radiation would reduce about 20% of the total cross section.

c) Other processes with double Higgs production in e^+e^- collisions have cross sections that are too small. Below we summarize the results of the cross section near to their maximum for the lowest Higgs mass, $M = 65$ GeV:

$e^+e^- \to \bar{t}tHH$ $\quad \sigma^{tot} = 0.0632\,\mathrm{fb}$ at $\sqrt{s} = 800\,\mathrm{GeV}$ and $m_{top} = 170$ GeV;
$e^+e^- \to W^+W^-HH$ $\quad \sigma^{tot} = 0.0346\,\mathrm{fb}$ at $\sqrt{s} = 700\,\mathrm{GeV}$;
$e^+e^- \to ZZHH$ $\quad \sigma^{tot} = 0.0043\,\mathrm{fb}$ at $\sqrt{s} = 610\,\mathrm{GeV}$;
$e^+e^- \to ZHHH$ $\quad \sigma^{tot} = 0.807 \cdot 10^{-3}\,\mathrm{fb}$ at $\sqrt{s} = 520\,\mathrm{GeV}$;
$e^\pm e^- \to e^\pm e^- HH$ $\quad \sigma^{tot} = 0.133\,\mathrm{fb}$ at $\sqrt{s} = 2\,\mathrm{TeV}$.

Only the last two reactions, where Higgs bosons are produced via ZZ fusion, are of some interest for light Higgs bosons. The reaction $ee \to ZHHH$ could be of special interest because this is the only place where the H^4 vertex contributes via the *Higgs - intermediate bosons* vertices. Unfortunately, the cross section is too small to observe it.

d) We found that for all processes with the *W-fusion* mechanism the energy distribution for outgoing particles has a universal behavior, as represented in Fig. 6 (not only for the e^+e^- collision, but also for the corresponding γe and $\gamma\gamma$ collisions). We see that Higgs bosons with $M_H < 300$ GeV are produced with relatively small energies, peaking at $\sim (M_H + M_W)$ (or even less). At the same time the energy of *spectator* neutrinos and/or W boson(s) has a high maximum at $\sim (\sqrt{s}/2 - M_H - M_W)$ and decreases abruptly to the point $\sim (\sqrt{s} - M_H)/2$. The remarkable feature is that the point $\sqrt{s}/4$ separates the energies of the spectators and Higgs bosons at about the 80% level for the W boson and the Higgs boson, and at 70% for the neutrino.

For the processes proceeding through the bremsstrahlung mechanism the energy distributions are similar for the Higgs and Z bosons. We point out only that the distribution for the Z boson is practically constant, while that for Higgs bosons increases slowly.

3.2 γe collisions

a) $\gamma e^- \to \nu_e W^- HH$. In this reaction Higgs bosons are produced via WW fusion (Fig. 5), in a way similar to the $ee \to \nu\nu HH$ case. The cross section increases with the energy. In total ten Feynman diagrams contribute to the unitary gauge (we do not count diagrams with *Higgs-electron* vertices due to a negligibly small coupling constant).

In Fig. 7 we give the angular distributions for the Higgs and W bosons. The Higgs distribution is symmetric. One can see that the W boson escapes mainly in directions close to the photon beam with a peak at $2^\circ - 3^\circ$ (for intermediate Higgs). The energy of the W boson is high, on the order of $(\sqrt{s}/2 - M_H - M_W)$ (see Fig. 6). Thus, about 90% of the events would have decay products of W going in a forward cone of 5°, and more than 50% within a cone of 2°. The signature with an additional W boson is free from any background. We conclude that the event selection has to be of two types: 1) with two additional high energy jets with invariant

mass peaking at M_W, 2) with a large missing energy, on the order of $(\sqrt{s}/2 - M_H - M_W)$, and missing transverse momentum ($> 10\,\mathrm{GeV/c}$). We also note that a number of events will include Higgs bosons escaping at angles of less than 15°.

We conclude that about 20 events per year can be observed for $M_H = 150$ GeV at $\sqrt{s_{\gamma e}} = 2$ TeV and $\mathcal{L} = 100\,\mathrm{fb}^{-1}/year$. The convolution with the photon spectrum decreases the cross section by three times for $M_H < 300$ GeV and $\sqrt{s_{ee}} = 2$ TeV. Since only left-handed electrons contribute in this reaction, the rate increases along with the rate of the longitudinal polarization of the electron beam. However, the dependence on the photon polarization is small, already only 3% at $\sqrt{s} \sim 1$ TeV.

b) $\gamma e \longrightarrow eZHH$. The total cross section is decreasing with the energy and Higgs mass. The maximum is $\sigma^{tot}_{max} = 0.009$ fb for $M_H = 65$ GeV at $\sqrt{s} = 500$ GeV. This cross section is too small to investigate experimentally.

3.3 $\gamma\gamma$ collisions

In $\gamma\gamma$ collisions double Higgs production is possible in several reactions at the tree level, and one process, $\gamma\gamma \to HH$, at the one-loop level. All of them are on the order of α^4.

a) $\gamma\gamma \longrightarrow WWHH$. In this reaction at high energies Higgs bosons are again produced via WW fusion (see Fig. 5). In total, thirty one Feynman diagrams contribute to the unitary gauge.

The total cross section increases with energy. The angular distribution is rather flat for Higgs bosons (see Fig. 7), while W bosons escape close to the collision axis, peaking at angles on the order of $3° - 4°$ (for intermediate Higgs). The energy distribution for W bosons has its maximum at $\sqrt{s}/2 - M_H - M_W$ (see Fig. 6). Hence, about 90% of the events would have decay products of W bosons going into forward or backward cones of 5°. If particle detection is not easy with such small escape angles, the triggering must include a large missing energy. It should be noted that the $\gamma\gamma \to HH$ reaction gives a background comparable to that of the signal, if only decay products of Higgs bosons are detected, but without missing energy. The reaction $\gamma\gamma \to WWHH$ is free from any background, except for incorrect combinatorial of jets; for $M_H < 150$ GeV the main branching is four b-jets (with an invariant mass peak at M_H) plus jets from two additional W bosons, up to four, and/or a large missing energy. In total, $8jet$ events can be detected. For $M_H > 150$ GeV the signature includes up to twelve quark jets with the invariant mass peaking at M_W and M_H.

Our conclusion is that for light and intermediate Higgs a visible number of events would be produced. For example, for $M_H = 150$ GeV about 20 events can be seen per year at PLC with $\sqrt{s_{\gamma\gamma}} = 2$ TeV and $\mathcal{L} = 100\,\mathrm{fb}^{-1}/year$, and about 14 events for $M_H = 200$ GeV.

The convolution with the photon spectrum decreases the cross section by $7 - 12$ times for $M_H = 100 - 200$ GeV. The dependence on the photons polarization is only 7% at $\sqrt{s} \sim 2$ TeV.

b) $\gamma\gamma \longrightarrow \bar{f}fHH$. Here, f is a fermion. Since the *Higgs-fermion* coupling is proportional to the fermion mass, we calculated only the t-quark case to estimate the upper bound for the cross sections. The total cross section decreases with energy, and has a maximum value of 0.07 fb at $M_H = 65$ GeV, $\sqrt{s_{\gamma\gamma}} = 850$ GeV and $m_{top} = 170$ GeV. Hence, this reaction can have visible statistics for only light Higgs, and a year integrated luminosity higher than $100\,\mathrm{fb}^{-1}$.

c) $\gamma\gamma \longrightarrow HH$. This reaction proceeds at the one-loop level. Analytical results for the

amplitudes and a detailed numerical analysis were carried out in [23]. In the range of Higgs masses discussed here the main features are the following. The cross-section dependence on the Higgs mass is weak for $M_H < 300$ GeV and $\sqrt{s} > 1$ TeV. The total cross section depends on the photon polarizations. There are two kinds of polarized cross sections: parallel ($\sigma^{++} = \sigma^{--}$) and anti-parallel, ($\sigma^{+-} = \sigma^{-+}$). In the parallel case the polarized cross section decreases very fast with energy, from ~ 0.6 fb at $\sqrt{s_{\gamma\gamma}} = 500$ GeV to ~ 0.02 fb at $\sqrt{s_{\gamma\gamma}} = 2$ TeV. At the same time σ^{+-} decreases very slowly, and is on the order of $0.5 - 0.3$ fb. We see that the rate of this reaction is comparable with that of *W-fusion* reactions. However, as shown in section 4, the sensitivity to the anomalous H^3 coupling is several times weaker for light and intermediate Higgs bosons.

3.4 $M_H = M_Z$ case

When the Higgs mass is equal to the Z mass, we cannot separate the Higgs signal from the Z background by reconstructing the jet-jet mass; b-tagging is useful to separate the Higgs signal for this case. It can be done by searching a second vertex from b-meson decay by a high-resolution vertex-detector. We assume that 80% b-tagging efficiency for the light-quark contamination is 0.5% and a c-quark 35% [24].

In the following analysis we require that at least two b-quarks are tagged for separating a double-H signal. The tagging efficiency for tagging two b-quarks out of four b-quarks from double-H production is 97%. The $Z \to b\bar{b}$ decay (15% branching ratio) and the miss-identification of $Z \to c\bar{c}$ (12% branching ratio) are taken into account. The background from a light-quark decay of Z is negligible. We should note that b-tagging would remove the possible background from W bosons due to a small branching ratio of $W \to cs$. We hereafter neglect the background from W bosons.

To study the $ee \to ZHH$ process we use a hadronic decay mode of the Z boson. A signal is of 6 jets (four b-quark jets from two Higgs bosons are expected). The background is the $ee \to ZZ\mathcal{B}$ processes, where $\mathcal{B}$ stands for Z or H. At a 500-GeV e^+e^- collider these processes have total cross sections of 1.15 fb and 0.95 fb, respectively, while the signal process has 0.305 fb. After b-tagging one can expect the ratio to be $S/B \sim 0.56$.

For $ee \to \nu\nu HH$ the background comes from the $ee \to \nu\nu Z\mathcal{B}$ process. At $\sqrt{s} = 2$ TeV their total cross sections are equal to 33.8 fb ($\mathcal{B} = Z$) and 6.48 fb ($\mathcal{B} = H$), while the signal process has 0.73 fb. Another background source also arises from the $ee \to eeZ\mathcal{B}$ processes with electrons and positrons being hidden in forward-backward invisible cones. Their total cross sections are equal to 4.65 fb ($\mathcal{B} = Z$) and 1.20 fb ($\mathcal{B} = H$). However, if we veto electrons in the visible region and apply a missing momentum cut at, for instance, several tens of GeV, we can reduce this background to less than 1/1000 with keeping the almost all signal events. Then we neglect these background hereafter. After the b-tagging one can expect the ratio to be $S/B \sim 0.13$.

For $\gamma e \to \nu WHH$ the background is $\gamma e \to \nu WZ\mathcal{B}$. Their cross sections were calculated to be $\sigma^{tot} = 31.1$ fb ($\mathcal{B} = Z$) and 4.49 fb ($\mathcal{B} = H$), respectively, at $\sqrt{s_{\gamma e}} = 2$ TeV, while the signal process has 0.361 fb. Here one can also expect only a very small ratio of $S/B \sim 0.12$ even with b-tagging.

For $\gamma\gamma \to WWHH$ the background is given by $\gamma\gamma \to WWZ\mathcal{B}$. The $\gamma\gamma \to WWZZ$ process has $\sigma^{tot} = 65.6$ fb[6] and 6.35 fb for $WWZH$ at $\sqrt{s_{\gamma\gamma}} = 2$ TeV, while the signal process has

[6]This result is in good agreement with [25] where it was calculated for the first time.

0.337 fb. Thus, $S/B \sim 0.06$ even with b-tagging.

Even if we apply a tighter cut for b-tagging, we cannot reduce the background from $Z \to b\bar{b}$ decay. The best value for the S/B ratio is given by $\sigma_{signal}/(\sigma_{BG}^{ZZ} * Br(Z \to b\bar{b})^2 + \sigma_{BG}^{ZH} * Br(Z \to b\bar{b}))$. The best values are 0.42, 0.26, and 0.14 for $ee \to \nu\nu HH$, $\gamma e \to \nu WHH$, and $\gamma\gamma \to WHH$, respectively. We need another method to separate H and Z events by using the angular distributions of their decay products [26]. However, this method also throws signal events away. We thus need higher luminosity colliders.

We may conclude that we must assume difficulties to observe double Higgs signals for $M_H \sim M_Z$ in *W-fusion* reactions. The situation is better for $ee \to ZHH$; one can hope that double light Higgs events can be detected even at a 500-GeV e^+e^- collider.

4 The δ-dependence

In this section we numerically analyze the sensitivity to the anomalous H^3 coupling. The numerical results for the parameters introduced in section 2 and their expected bounds are summarized in Table 1. We also show some representative curves in Figs. 8 and 9.

One can see a large difference between $ee \to ZHH$ and other reactions associated with different Higgs-boson production mechanisms in *bremsstrahlung* (Fig. 3) and *W-fusion* (Fig. 5), respectively.

In all cases the minimum point (δ_0) eventually moves to the SM point $\delta = 0$ when the Higgs mass increases. We illustrate this in Fig. 8. However, we observe that δ_0 moves in the opposite directions in fusion and bremsstrahlung cases. The SM point is still rather far from δ_0 for $ee \to ZHH$, while in the fusion cases the SM point reaches δ_0 at $M_H = 300$ GeV for $ee \to \nu\nu HH$, at $M_H = 250$ GeV for $\gamma e \to \nu WHH$ and already at $M_H = 200$ GeV for $\gamma\gamma \to WWHH$.

In Table 1 the upper and lower bounds of the δ ($\delta^{\pm}$) are shown for year-integrated luminosity, $\mathcal{L}_y = 100\,\mathrm{fb}^{-1}$. One can see the change of modes from (A) to (B) (see the section 2) at the points $M_H \sim 200$ GeV for $ee \to ZHH$ and $M_H \sim 110$ GeV for $ee \to \nu\nu HH$. This critical point depends on the luminosity; for example, for $\mathcal{L}_y = 10\,\mathrm{fb}^{-1}$ in the reaction $ee \to ZHH$ this point is $M_H \sim 70$ GeV.

a) **Light Higgs**. In the process $ee \to ZHH$ for $M_H = 65$ GeV at a 500-GeV e^+e^- collider the limitations are $\delta^- \sim -4.0$ and $\delta^+ \sim 1.8$. The effect of discrete uncertainty is seen (see section 2) with a *shadow* interval $\sim (-10.2, -4.4)$. Since these two intervals are very close to each other, the real bounds would be about $-10 < \delta < 1.8$. In the $M_H \sim M_Z$ case we have to recall the large background, $S/B \sim 0.56$ (see section 3.1), and note that an integrated luminosity of $10\,\mathrm{fb}^{-1}/year$ (3 signal events per year) would not be sufficient for establishing limitations on δ.

At $\sqrt{s} = 2$ TeV and $\mathcal{L}_y = 100\,\mathrm{fb}^{-1}$ the possible limitations on δ for $M_H = 65$ GeV are $-0.42 < \delta < 0.61$ in $ee \to \nu\nu HH$. Here, the effect of a discrete uncertainty shows up rather clearly, and the *shadow* interval is $\sim (2.4, 3.4)$. We see that the $ee \to \nu\nu HH$ reaction is better for determining δ, particularly for the upper bound, (δ^+). We have to mention that due to poor statistics and a very small signal-to-background ratio the case $M_H \sim M_Z$ is practically beyond the scope of experimental plausibility to probe the anomalous H^3 coupling at future linear colliders at the TeV energy range in *W-fusion* reactions.

b) **Intermediate Higgs**. First, one can see that a 500-GeV e^+e^- collider has no feasibility

for these Higgs masses in all *W-fusion* processes (see Fig. 1). However, for a small area, $M_H < 100$ GeV, the reaction $ee \to ZHH$ can give some limitations: for $M_H = 100$ GeV and $\mathcal{L}_y = 10\,\text{fb}^{-1}$ the bounds are obtained as $\delta^- = -8.1$ and $\delta^+ = 2.0$.

For a linac with $\sqrt{s} = 2$ TeV and $\mathcal{L}_y = 100\,\text{fb}^{-1}$ we have the following results. First the lower bound (δ^-) is practically independent of the reaction type (*W-fusion* ones) and the Higgs mass. It is given by $\delta^- \sim -0.3$. As for the upper bound δ^+ the reaction $ee \to \nu\nu WW$ is better for $M_H < 110$ GeV where $\delta^+ \sim 0.6$. In this case a discrete uncertainty appears with a *shadow* interval of $\sim (1.3, 2.2)$; however this uncertainty can be resolved with the help of the $\gamma\gamma$ reaction. For heavier masses the $\gamma\gamma$ reaction is the best variant to give the limitations at the $\delta^+ \sim 0.85 - 0.36$ level for $M_H = 120 - 200$ GeV.

We also note that if the PLC luminosity can be increased (for example, as discussed in [8, 11]) the $\gamma\gamma$ reaction can set a strict limit on δ. In the case of $\mathcal{L}_y^{PLC} \sim 10^4\,\text{fb}^{-1}$, although these bounds can be established at the $\delta^- \sim -0.05$ and $\delta^+ \sim 0.08$ level, they appear together with a *shadow* interval of $\sim (0.2, 0.35)$.

c) **Heavy Higgs**. We have found that in the *W-fusion* cases the dependence of the cross sections on the Higgs mass is changed if δ is sufficiently large. We show some representative curves for three values of H^3 anomalous coupling in Fig. 9. This effect can be explained by the competition of two factors. One factor is associated with decreasing the total phase space volume by large Higgs masses; the other is associated with increasing the phase volume where the Higgs propagator can be regarded as being constant. For a larger δ the second factor becomes significant. Thanks to this effect anomalous H^3 coupling in *W-fusion* processes becomes detectable for rather large masses. For example, the value $|\delta| = 1$ allows measurements up to $M_H = 750$ GeV at a linac with $\sqrt{s} = 2$ TeV in the $ee \to \nu\nu HH$ reaction. For such high Higgs masses the unpolarized total cross section is $\sigma^{tot}(\delta = \pm 1) > 0.015$ fb, while the SM cross section is negligible. In the $\gamma\gamma \to WWHH$ reaction a measurement of $\delta = 1$ is possible up to $M_H \sim 800$ GeV when $\sigma^{tot}(\delta = 1) \sim 0.02$ fb.

d) $\gamma\gamma \to HH$. Finally, we present some basic numbers for the $\gamma\gamma \to HH$ reaction using the results from [23]. The important point is that anomalous H^3 coupling contributes only to amplitudes with equal photon polarizations. However, for such polarizations and for $M_H < 300$ GeV the cross section is dominated by diagrams with a t-quark loop, more than 90% for $\sqrt{s} = 500$ GeV and $\sim 100\%$ for $\sqrt{s} > 1$ TeV. Consequently, we have here a different origin for the δ dependence from tree level reactions. As a result, the sensitivity to δ is several-times weaker in this reaction compared with that in *W-fusion*. For example, from the figures presented in [23] one can pick out the following cross sections for $M_H = 250$ GeV: $\sigma^{tot}(\delta = 0) \sim 0.104$ fb, $\sigma^{tot}(\delta = -1) \sim 0.112$ fb and $\sigma^{tot}(\delta = 1) \sim 0.1$ fb. These results were obtained at $\sqrt{s_{ee}} = 2$ TeV along with a convolution of the photon energy spectrum. Due to this convolution the cross section does not show any large change for relatively light Higgs masses (< 300 GeV). Hence, the possible limitations are $\delta^- \sim -4.3$ and $\delta^- \sim 7.3$. Such a weak sensitivity means that the interaction of the Higgs boson with the W boson has a stronger dependence on the anomalous H^3 coupling than does an interaction with fermions. This difference is certainly associated with the fact that the *Higgs-W* interaction is deeply involved in the mechanism of a spontaneous breaking of the local gauge invariance (in the case of anomalous coupling also). One can find a supporting argument in the figures presented in [23]. In fact, for $M_H > 500$ GeV and $\sqrt{s} > 1$ TeV the main contribution to the amplitudes with equal photon polarizations comes from the W-loop diagrams; in this mass range the sensitivity on δ is significantly increased.

5 Conclusions

The 500-GeV e^+e^- collider will have some possibility to observe double Higgs production and probe anomalous H^3 coupling for only light Higgs boson. An experimental study is feasible for the $ee \to ZHH$ reaction with statistics of more than 5 events per year. The anomalous coupling may be bounded at the $-10 < \delta < 2$ level. In this reaction, even for the $M_H \sim M_Z$ case, a number of events can be separated from the background.

Stronger limitations on the anomalous H^3 coupling for light or intermediate Higgs bosons can be expected at a linac with ~ 2 energy TeV and a year-integrated luminosity of $\sim 100\,\mathrm{fb}^{-1}$. All three options ($e^+e^-$, γe and $\gamma\gamma$) are plausible for a experimental studies of reactions induced by the *W-fusion* mechanism: $ee \to \nu\nu HH$, $\gamma e \to \nu WHH$ and $\gamma\gamma \to WWHH$. For the light Higgs boson limitations on the order of $-0.4 < \delta < 0.6$ are possible in $ee \to \nu\nu HH$ the reaction. For the intermediate Higgs boson in the SM the rates are more than 30 events per year for $ee \to \nu\nu HH$ and more than 20 events for γe and $\gamma\gamma$. However, the dependence on anomalous H^3 coupling is stronger in $\gamma\gamma \to WWHH$, where the limitations can be established at the $-0.3 < \delta < 0.6$ level for $M_H \sim 100$ GeV and $-0.3 < \delta < 0.36$ for $M_H \sim 200$ GeV. Anomalous $\delta = \pm 1$ couplings will be measured up to $M_H \sim 700 - 800$ GeV in reactions with *W-fusion*.

Probing the anomalous H^3 coupling for $M_H \sim 1$ TeV and heavier is possible only in the $\gamma\gamma \to HH$ [23] reaction.

The last conclusion is that if the luminosity of the PLC is much higher compared with that of the basic linac (in $10 - 100$ times), $\gamma\gamma \to WWHH$ should give the best limitations at a level of less than $|\delta| < 0.1$.

Acknowledgements

This work was supported in part by the Japan Society for the Promotion of Science. V.A.I. and A.E.P. were supported also by European association INTAS (project 93-1180) and International Science Foundation (grants M9B000 and M9B300). We are also indebted to KASUMI Co. Ltd. and SECOM Co. Ltd. for the financial support to our collaboration.

V.A.I. expresses his deep gratitude to Minami-Tateya collaboration (KEK) for hospitality and for providing him with excellent conditions to stay and work in Japan.

References

[1] M. Pohl, *Proceedings of 27th Int. Conf. on High Energy Physics* (Glasgow, July 20-27, 1994), p.107, ed. P.J. Bussey and I.G. Knowls.

[2] See, for example, articles in: *Physics and Experiments with Linear Colliders*, ed. R. Orava, P. Eerola and M. Nordberg (World Scientific, Singapore, 1992);
Proc. Workshop 'e^+e^- collisions at $500GeV$*: the physics potential'*, ed. P.W. Zerwas, DESY 92-123A (1992);
'JLC-I', KEK-Report 92-16 (1992).

[3] J.F. Gunion, H.E. Haber, G. Kane and S. Dawson, *The Higgs Hunter's Guide* (Addison-Wesley, 1990).

[4] A. Djouadi, J. Kalinowski and P.W. Zerwas, in: *Proc. Workshop 'e^+e^- collisions at 500GeV: the physics potential'*, ed. P.W. Zerwas, DESY 92-123A (1992) p.83.

[5] I.F. Ginzburg, G.L. Kotkin, V.G. Serbo and V.I. Telnov, Pis'ma Zhh. Eksp. Teor. Fiz. **34** (1981) 514; Nucl. Instr. Methods **205** (1983) 47.
I.F. Ginzburg et al., Nucl. Instr. Methods **219** (1984) 5.

[6] E.L. Saldin et al., DESY 94-243, December 1994.

[7] We are grateful to I.F.Ginzburg for the discussion of this point. The corresponding references are [5, 8, 9]. Recent discussion has been concluded [10] that PLC luminosity can be 1/5 - 1/3 of basic linac with practically monochromatic photon beam. We refer also to [8, 11] where an idea to increase PLC luminosity up to $10^{35} - 10^{36}\,\mathrm{cm}^{-2}\mathrm{s}^{-1}$ is described.

[8] V.I. Telnov, Nucl. Instr. Methods **A294** (1990) 72.

[9] I.F. Ginzburg, Nucl. Phys. B (Proc. Suppl.) **37B** (1994) 303.
I.F. Ginzburg, G.L. Kotkin, V.G. Serbo and V.I. Telnov, Phys. Rep. **C** (to be appeared).

[10] *10th Workshop on Photon-Photon Collisions (Photon'95)* (Sheffield, England, April 8-13, 1995).

[11] V.I. Telnov, in: *Proc. Workshop on Physics and Experiments with Linear e^+e^- Colliders*, vol. II, ed. F.A. Harris et al. (World Scientific, Singapore, 1993) p.551; Nucl. Instr. Methods **A355** (1995) 3.
V.E. Balakin and N.A.Solyak, Nucl. Instr. Methods **A355** (1995) 142.
V.E. Balakin and A.A.Sery, Nucl. Instr. Methods **A355** (1995) 157.

[12] T. Maruyama et al., Phys. Rev. Lett. **66** (1991), 2351,
T. Omori et al., *Proc. of High Energy Accelerator Conference, Hamburg 1992*, (World Scientific, Singapore, 1992), Vol-I, p.157,
H. Aoyagi et al., Phys. Lett. **A167** (1992), 415,
Y. Kurihara et al., Jpn. J. Appl. Phys. **34** (1995), 355.

[13] For a helical undulater method, see V.E. Balakin, A.A. Mikhailichenko, INP 79-85(1979), K. Flöttmann, DESY 93-161(1993).
For the other methods, see M. Chiba et al., in *Proceedings of the fifth JLC workshop*, ed. Y. Kurihara.

[14] G.J. Gounaris, D. Schildknecht and F.M Renard, Phys. Lett. **83B** (1979) 191.

[15] V. Barger, T. Han and R.J.N. Philips, Phys. Rev. **D38** (1988) 2766.

[16] V. Barger and T. Han, Mod. Phys. Lett. **A5** (1990) 667.

[17] An analogous procedure was used in [18] so as to see the contribution of higher order monomials for heavy Higgs ($M_H \sim 1$ TeV and more).

[18] J.J. van der Bij, Nucl. Phys. **B267** (1986) 557.

[19] E.E. Boos et al., Preprint INP MSU-94-36/358, SNUTP 94-116, Seoul, 1994; hep-ph/9503280.

[20] GRACE Manual, v.1.0, KEK Report 92-19, 1993.

[21] E.E. Boos et al., Int. J. Mod. Phys. **C5** (1994) 615.

[22] K.J.F Gaemers and F. Hoogeveen, Z. Phys. **C26** (1984) 249.

[23] G. Jikia and A. Tkabladze, in: *Proc. Workshop 'e^+e^- collisions at* $500GeV$*: the physics potential'*, ed. P.W. Zerwas, DESY 93-123C (1993) p.529.

[24] N. Brown, Z. Phys. **C49** (1991) 657.
'JLC-I', KEK-Report 92-16 (1992) p.86.
P. Grosse-Wiesmann, D. Haidt and J. Schreiber, in *Proc. Workshop 'e^+e^- collisions at* $500GeV$*: the physics potential'*, ed. P.W. Zerwas. DESY 92-123A (1992) p.37.

[25] G. Jikia, IHEP 94-77, hep-ph/9407393, July 1994; Nucl. Phys. **B437** (1995) 520.
K. Cheung, Phys. Rew. **D50** (1994) 4290.

[26] Z. Kunszt and W. Stirling, Phys. Lett. **B242** (1990) 502.

Tables captions

Table 1: Total cross sections and parameters representing the dependence on the anomalous H^3 coupling. Calculations with unpolarized beams. For the γe and $\gamma\gamma$ channels the results are obtained for monochromatic photon beam(s).

Figures captions

Figure 1: Energy dependence of the unpolarized monochromatic total cross sections in the SM: 1) $ee \to ZHH$; 2) $ee \to \nu\nu HH$; 3) $\gamma e \to \nu WHH$; 4) $\gamma\gamma \to WWHH$.

Figure 2: Unpolarized monochromatic total cross section as a function of the Higgs mass in the SM. The curves correspond to the same processes as in Fig. 1. For $ee \to ZHH$ σ^{tot}_{max} is calculated at the corresponding energies; these points are represented as a curve. For other processes the curves are obtained at $\sqrt{s} = 2$ TeV.

Figure 3: Feynman diagrams for $e^+e^- \to ZHH$ (diagrams with *Higgs-electron* vertices are not represented due to negligible coupling constant).

Figure 4: Higgs angular distributions in SM: 1) $ee \to ZHH$ at $M_H = 65$ GeV and $\sqrt{s} = 335$ GeV; 2) $ee \to \nu\nu HH$ at $M_H = 150$ GeV and $\sqrt{s} = 2$ TeV. For both distributions 5000 events were generated.

Figure 5: Feynman diagrams for the fusion mechanism $WW \to HH$ for double Higgs production. For the discussed processes virtual incoming W bosons are suspended to the initial electron (positron) or photon.

Figure 6: Energy distribution for *out* particles for reactions involving the *W-fusion* mechanism. Here $x \equiv 2E/\sqrt{s}$ and x_{max} corresponds to the distribution maximum. For Higgs bosons $x_0 = 2M_H/\sqrt{s}$, $x_{max} < 2(M_H + M_W)/\sqrt{s}$ and $x_1 \sim 1 - 2M_W/\sqrt{s}$. For the spectators, $x_0 = 0$ (for neutrino) or $2M_W/\sqrt{s}$ (for W boson), $x_{max} \sim 1 - 2(M_H + M_W)/\sqrt{s}$ and $x_1 \sim 1 - M_H/\sqrt{s}$. This picture is typical for $\sqrt{s} \sim 2$ TeV and $M_H = 100 - 300$ GeV.

Figure 7: Angular distributions in SM for $\gamma e \to \nu WHH$ (left side) and $\gamma\gamma \to WWHH$ (right side). For all distributions 5000 events were generated.

Figure 8: Dependence of unpolarized σ^{tot} on the H^3 anomalous coupling for $\gamma\gamma \to WWHH$.

Figure 9: Unpolarized σ^{tot} *vs* Higgs mass: left side for $ee \to \nu\nu HH$; right side for $\gamma\gamma \to WWHH$.

Table

Process	M_H	Cross sections			δ_0	$\hat{\mathcal{L}}$	δ^-	δ^+
	GeV	$\delta=0$ (SM)	$\delta=-1$	$\delta=1$		fb^{-1}	($\mathcal{L}=100\,$fb^{-1})	
		σ^{tot}_{max} fb (at $\sqrt{s}$ TeV)						
	65	0.61 (0.335)	0.41	0.87	-4.2	9	-0.73	0.62
	M_Z	0.32 (0.44)	0.20	0.49	-3.3	21	-0.88	0.69
$e^+e^- \to$	120	0.20 (0.56)	0.12	0.32	-2.9	36	-1.1	0.77
ZHH	150	0.14 (0.7)	0.079	0.23	-2.5	58	-1.3	0.82
	200	0.094 (0.95)	0.050	0.17	-2.0	109	-4.8	0.85
	250	0.072 (1.2)	0.036	0.13	-1.8	143	-4.4	0.86
	300	0.059 (1.5)	0.029	0.12	-1.6	180	-4.1	0.85
		σ^{tot} fb at $\sqrt{s}=2$ TeV						
	65	1.0	1.6	0.77	1.5	42	-0.42	0.61
	M_Z	0.73	1.4	0.52	1.0	64	-0.34	0.55
$e^+e^- \to$	120	0.49	1.2	0.41	0.64	133	-0.30	1.6
$\bar{\nu}_e\nu HH$	150	0.34	0.99	0.37	0.45	262	-0.28	1.2
	200	0.19	0.81	0.40	0.25	1116	-0.27	0.77
	250	0.11	0.67	0.41	0.15	4871	-0.27	0.56
	300	0.066	0.55	0.41	0.086	$>10^4$	-0.27	0.44
	65	0.51	0.86	0.37	1.1	100	-0.47	2.8
	M_Z	0.36	0.78	0.28	0.73	169	-0.38	1.8
$\gamma e \to$	120	0.26	0.71	0.27	0.47	381	-0.33	1.3
$\nu_e WHH$	150	0.19	0.65	0.31	0.30	1088	-0.32	0.91
	200	0.11	0.58	0.38	0.13	$>10^4$	-0.31	0.58
	250	0.072	0.51	0.44	0.047	$>10^4$	-0.32	0.41
	300	0.048	0.45	0.45	-0.0012	$>10^4$	-0.33	0.33
	65	0.46	0.86	0.38	0.76	213	-0.43	1.9
	M_Z	0.34	0.86	0.36	0.47	370	-0.34	1.3
$\gamma\gamma \to$	120	0.25	0.86	0.43	0.28	1102	-0.30	0.85
$WWHH$	150	0.20	0.86	0.55	0.15	5817	-0.29	0.59
	200	0.13	0.84	0.76	0.028	$>10^4$	-0.30	0.36
	250	0.10	0.80	0.92	-0.038	$>10^4$	-0.33	0.25
	300	0.08	0.75	0.99	-0.078	$>10^4$	-0.35	0.20
	500	0.033	0.36	0.61	-0.14	1641	-0.45	0.17

Table 1:

Figures

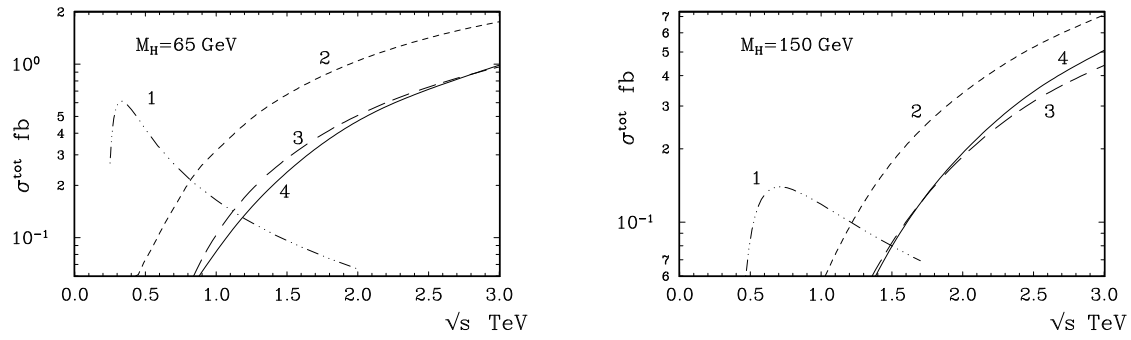

Figure 1:

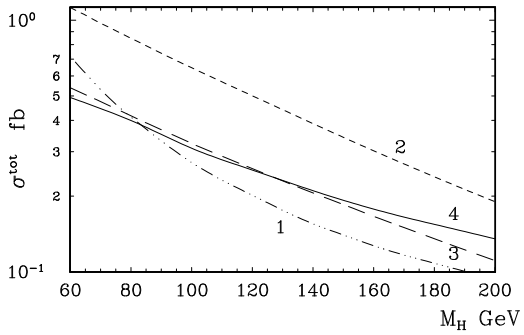

Figure 2:

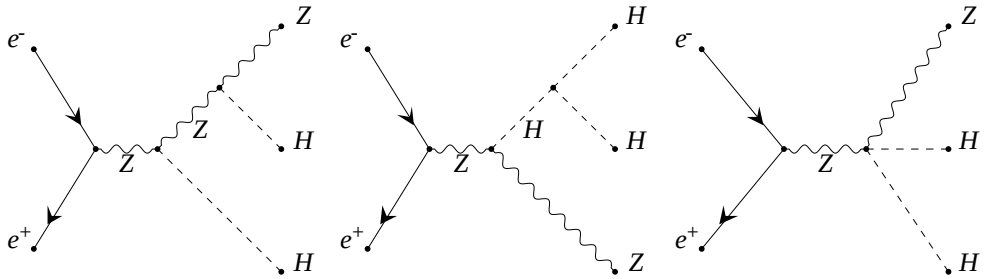

Figure 3:

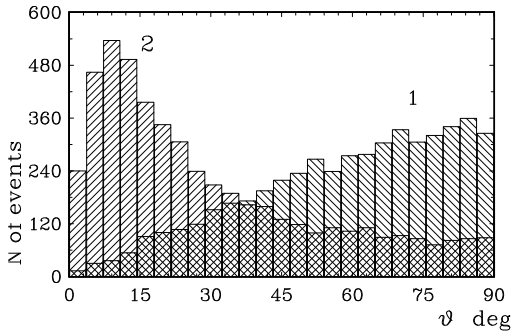

Figure 4:

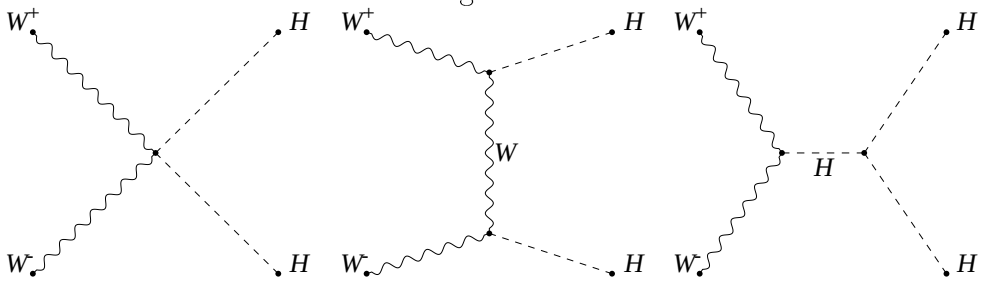

Figure 5:

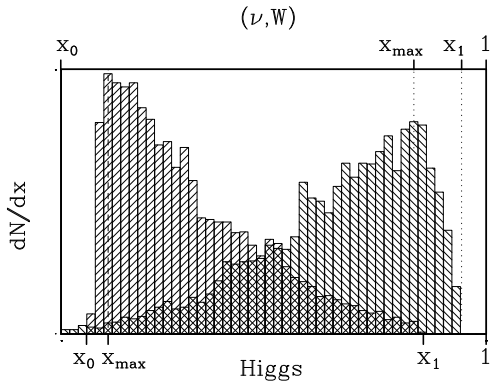

Figure 6:

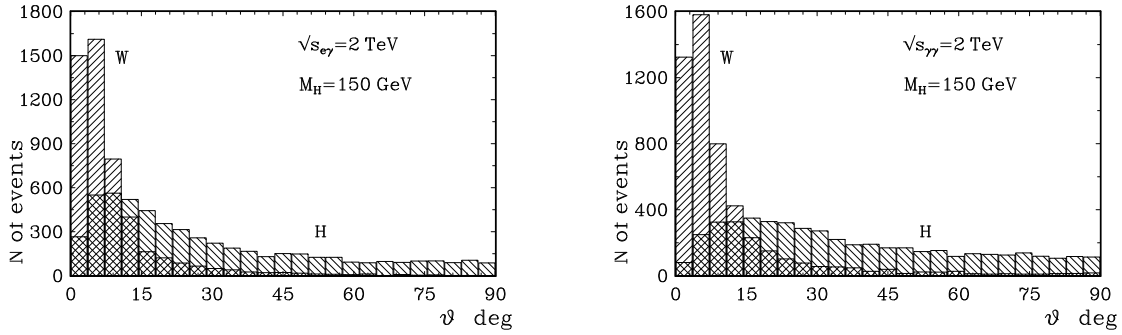

Figure 7:

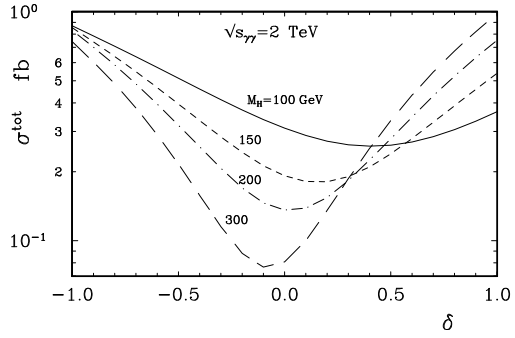

Figure 8:

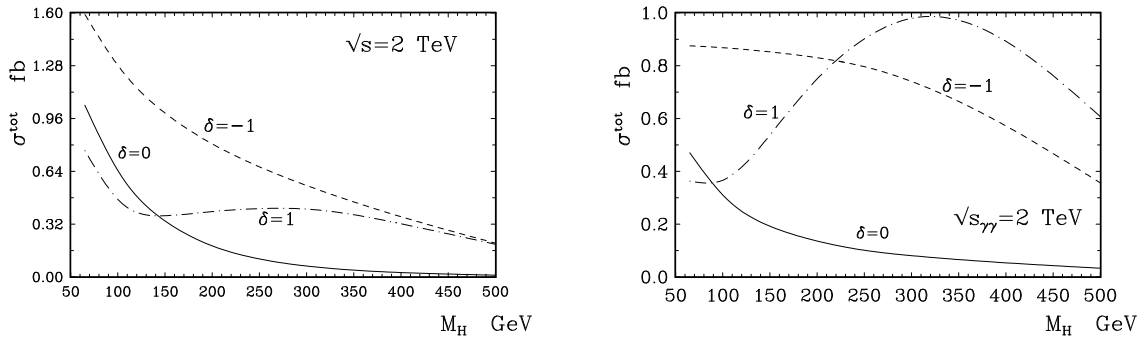

Figure 9: